Chapter 2
Theory and Applications of the Fast Lyapunov Indicator (FLI) Method

Elena Lega, Massimiliano Guzzo, and Claude Froeschlé

Abstract In the last 20 years numerical experiments have allowed to study dynamical systems in a new way providing interesting results. The development of tools for the detection of regular and chaotic orbits has been one of the key points to access the global properties of dynamical systems. In many cases the visualization of suitably chosen sections of the phase space has been determinant for the comprehension of the fascinating and complex interplay between order and chaos. The Fast Lyapunov Indicator introduced in Froeschlé et al. (Celest Mech Dyn Astron 67:41–62, 1997) and further developed in Guzzo et al. (Physica D 163(1–2):1–25, 2002), is an easy to implement and sensitive tool for the detection of order and chaos in dynamical systems. Closely related to the computation of the Largest Lyapunov Exponent, the Fast Lyapunov Indicator relies on the idea that the computation of tangent vectors contains a lot of information even on short integration times, while for the Largest Lyapunov Indicator large integration times are required in order to accurately approximate a limit value. The aim of this Chapter is to provide the definition of the Fast Lyapunov indicator and some simple examples of applications for readers that would like to implement and use the indicator for the first time. We associate to each example of application the references to more specific papers that we have published during these years.

E. Lega (✉)
Université de Nice Sophia Antipolis, CNRS UMR 7293, Observatoire de la Côte d'Azur, Bv. de l'Observatoire, CS 34229, 06304 Nice cedex 4, France
e-mail: elena@oca.eu

M. Guzzo
Dipartimento di Matematica, Università degli studi di Padova, Via Trieste, 63 - 35121 Padova, Italy
e-mail: guzzo@math.unipd.it

C. Froeschlé
Université de Nice Sophia Antipolis, CNRS UMR 7293, Observatoire de la Côte d'Azur, Bv. de l'Observatoire, B.P. 4229, 06304 Nice cedex 4, France
e-mail: claude@gmail.com

Ch. Skokos et al. (eds.), *Chaos Detection and Predictability*, Lecture Notes in Physics 915, DOI 10.1007/978-3-662-48410-4_2

2.1 Introduction

The study of the interplay between order and chaos is one of the keys for understanding the behaviour of complex systems. Since the pioneering work of Hénon and Heiles [27] the use of numerical simulations together with the development of different tools for the detection of chaos has provided interesting results in different domains of physics (celestial mechanics, particle accelerators, dynamical astronomy, statistical physics, plasma physics).

In their study, Hénon and Heiles, searching for the existence of a third integral of motion in a galactic potential, were surprised by finding that ordered and chaotic motions co-existed for some values of the total energy of the system. As usual in numerical experiments the authors searched for eventual numerical errors. Listening to a seminar by Arnold about new theoretical results on stability of quasi-integrable Hamiltonian systems (the nowadays celebrated KAM theorem [1, 28, 43]), M. Hénon understood that order and chaos are complementary rather than antagonist dynamical behaviours and got convinced on the numerical results he had obtained with C. Heiles in their study of the galactic potential. Since then, numerical experiments have become a sort of laboratory, very often used to extend the domain of validity of theorems and therefore showing their interest for physical problems.

As an example, we consider the problem of the long term stability properties of a dynamical system, problem of particular interest in the domain of celestial mechanics. During the last decade the numerical detection of the resonances of a system using dynamical indicators has been one of the major tools for studying the long-term stability in the specific case of celestial mechanics (for recent examples, see [15, 16, 29, 42, 49–51, 55]). The reason is that many problems of interest for celestial mechanics can be studied with KAM [1, 28, 43] and Nekhoroshev theorems [48]. For small values of the perturbation parameters the KAM theorem leaves the possibility of large instabilities only on a peculiar subset of the phase space, the so-called Arnold web. According to the Nekhoroshev theorem, on the Arnold web the diffusion times are expected to increase at least exponentially with an inverse power of the norm of the perturbation. This phenomenon of extremely slow diffusion was introduced by Arnold [2] on an ad-hoc model well suited to the mathematical demonstration rather than for numerical experiments.

We recall that, for many years, researchers were convinced that Arnold's diffusion could not be detected numerically, and therefore, in some sense, the phenomenon was not interesting for the study of physical systems.

The Fast Lyapunov Indicator (FLI hereafter), introduced in [12] and further developed in [21], is an easy (to implement) and sensitive tool for the detection of the Arnold web of a system. The FLI method was first tested by comparing results obtained with other chaos indicators. A detailed comparison with the frequency analysis application on two and four dimensional mapping [30, 31] can be found in [10, 32]. The comparison with other chaos indicators was presented in [33]. Without entering in the details, we can say that the FLI belongs to the class of the so called

finite time chaos indicators (such as the Finite Time Lyapunov Exponent [52], the MEGNO [8, 9] as well as OFLI and OFLI2 [3]) which are able to discriminate between regular orbits and chaotic orbits on times significantly smaller than the time required for a reliable estimation of the largest characteristic Lyapunov exponent or of the frequency.

The detailed detection of the resonances obtained with the FLI on models which satisfy the hypothesis of both KAM and Nekhoroshev theorems allowed us to measure directly the quantitative features of the Arnold's diffusion [14, 18, 22–26, 35, 36, 53] showing its interest for physical systems. Later in [17, 24, 37–40] we have used the FLI for the detection of the stable and unstable manifolds. More recently the FLI has been applied to the planar circular restricted three body problem for the detection and characterization of close encounters and resonances [19, 41]; more precisely, we have formulated the FLI method using the Levi–Civita regularization in order to handle the singularity of the gravitational potential.

The majority of our studies concern conservative systems, however, we have used the FLI for studying the dynamics of dissipative systems in [5–7]; more recently we have provided an application of the FLI to track the diffusion of orbits of a quasi integrable Hamiltonian system perturbed with a very small non-Hamiltonian perturbation [18].

In this Chapter, rather than providing a review of the results obtained with the FLI, we present the indicator for readers that would like to implement it for the first time. At this purpose we provide in Sect. 2.2 the definition and use of the FLI on a simple 2-dimensional discrete model: the standard map. On this model we try to answer to some frequently asked questions about the implementation and use of the method. In Sect. 2.3 we show the use of the FLI for the computation of the stable and unstable manifolds. In Sect. 2.4 we provide an application on a generic Hamiltonian model. In Sect. 2.5 we show an application of the FLI for the detection of the resonances of a quasi-integrable Hamiltonian system with 3 degrees of freedom and we show how to use the FLI to follow the diffusion of orbits along resonant lines. Conclusions are provided in Sect. 2.6.

2.2 Definition of the Fast Lyapunov Indicator

Given a set of differential equations:

$$\frac{dx}{dt} = F(x) \ , \ x = (x_1, x_2, ...x_n) \tag{2.1}$$

for any solution $x(t)$ with initial condition $x(0)$ the evolution $v(t)$ of any tangent vector with initial value $v(0)$ is obtained by integrating the variational equations:

$$\begin{cases} \frac{dx}{dt} = F(x) \\ \frac{dv}{dt} = \frac{\partial F}{\partial x} v. \end{cases} \tag{2.2}$$

If instead one considers the discrete-time dynamics defined by the map

$$x(t+1) = \psi(x(t)), \tag{2.3}$$

the evolution of the tangent vector is defined by:

$$\begin{cases} x(t+1) = & \psi(x(t)) \\ v(t+1) = & \frac{\partial \psi}{\partial x}(x(t))v(t). \end{cases} \tag{2.4}$$

With this setting, for both systems (2.1) and (2.3), the simplest definition of the fast Lyapunov indicator of a point $x(0)$ and of a tangent vector $v(0)$, at time t, is:

$$\mathrm{FLI}_t(x(0), v(0)) = \log \frac{\|v(t)\|}{\|v(0)\|} \,. \tag{2.5}$$

The FLI is defined in such a way that, unless $v(0)$ belongs to some lower dimensional linear spaces, the quantity $\mathrm{FLI}_t(x(0), v(0))/t$ tends to the largest Lyapunov exponent as t goes to infinity. If Eq. (2.1) is Hamiltonian and if the motion is regular (except for some peculiar hyperbolic structures, such as whiskered tori) then the largest Lyapunov exponent is zero, otherwise it is positive. This property has been largely used to discriminate between chaotic and ordered motions. However, among regular motions the Lyapunov exponent does not distinguish between circulation and libration orbits. In contrast, the FLI distinguishes between them ([13, 34], see Sect. 2.1).

Therefore, the computation of $\mathrm{FLI}_t(x, v)$ on grids of initial conditions x and for the same fixed tangent vector v allows one to detect the distribution of invariant tori and resonances (i.e. circulation and libration orbits) in relatively short CPU times [11, 13].

We remark that the FLI depends parametrically on the initial vector $v(0)$ and on the integration time t. A frequently asked question concerns the choice of $v(0)$ for the practical implementation of the method. As for the computation of the largest Lyapunov exponent, one has in principle to avoid special choices of $v(0)$. In order to reduce the dependence of the computation on the choice of the initial tangent vector we suggested in [18] to compute the average (or alternatively the maximum) of the FLIs obtained for an orthonormal basis of tangent vectors. It happens that any orthonormal basis is suitable to detect the dynamics of the system. A second frequently asked question concerns the choice of the integration time t. We answer to both questions in the following using the standard map as a model problem.

2.2.1 The Standard Map as a Model Problem

We consider as a model problem the two-dimensional standard map, whose phase space variables are denoted by $(I, \varphi) \in \mathbb{R} \times \mathbb{S}^1$, and whose dynamics is defined by

$$(I(t+1), \varphi(t+1)) = \psi(I(t), \varphi(t)) \tag{2.6}$$

with

$$\psi(I, \varphi) = (I + \epsilon \sin(\varphi + I), \varphi + I),$$

and ϵ is a parameter. As it is well known, the map has interesting dynamics for $\epsilon \neq 0$. As an example, in Fig. 2.1, we report the phase-portrait of the map for $\epsilon = 0.3$: we can appreciate the presence of invariant curves, as well as of a small chaotic zone around the hyperbolic fixed point $(0, 0)$. We select three initial conditions on the phase-portrait of Fig. 2.1, according to different dynamical features: we select an initial condition in the small chaotic region around the origin, a second one corresponding to a resonant libration and finally a third one corresponding to a circulation curve (see Fig. 2.1). In Fig. 2.2 we report the time evolution of the FLI for the three orbits. We remark that about 10 iterations of the map are enough to differentiate the chaotic orbit, whose tangent vector growths approximately exponentially with time, from the regular libration and circulation, whose tangent vectors increase almost linearly with time (correspondingly, the FLI increases almost linearly with time for the chaotic orbit, and approximately logarithmically for the regular motions).

In order to reduce the fluctuations that appear on Fig. 2.2 one can conveniently compute, instead of the indicator defined in (2.5), the indicator:

$$\mathrm{FLI}(x(0), v(0), t) = \sup_{0 \leq k \leq t} \log ||v(k)|| \tag{2.7}$$

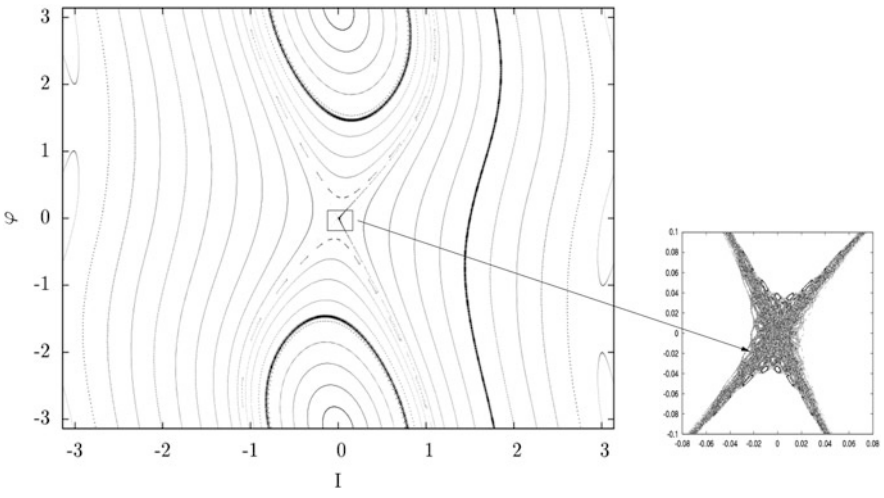

Fig. 2.1 *On the left*: a set of orbits of the standard mapping for $\epsilon = 0.3$. The *black points* correspond to a resonant libration orbit of initial conditions $(I(0), \varphi(0)) = (0, 1.5)$ and to a circulation orbit of initial conditions $(I(0), \varphi(0)) = (1.5, 0)$. *On the right*: enlargement around the hyperbolic fixed point at $I(0) = 0, \varphi(0) = 0$

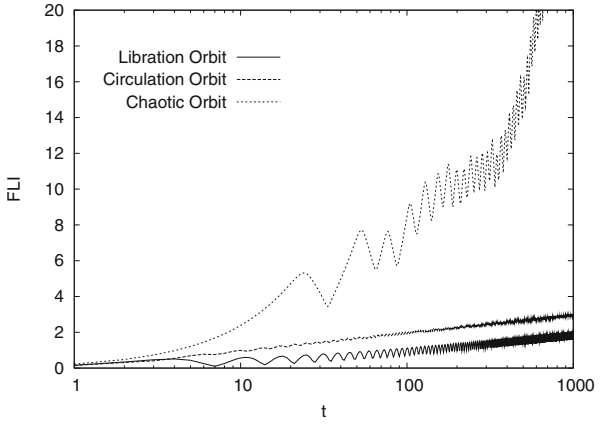

Fig. 2.2 Evolution with time of the FLI for the standard map of Eq. (2.6) for $\epsilon = 0.3$ for 3 orbits of initial conditions $(10^{-5}, 0)$ corresponding to the small chaotic region around the hyperbolic fixed point at the origin (right panel of Fig. 2.1), $(0, 1.5)$ and $(1.5, 0)$ corresponding respectively to the libration orbit and to the circulation curve marked with points in Fig. 2.1

Figure 2.3 shows that computing the FLI as in (2.7) the fluctuations become negligible. We remark that, while the Largest Lyapunov exponent is zero for both libration and circulation orbits, their corresponding FLI are different. In fact, using a refined perturbation theory we have shown in [21] that the value of the FLI differs at order 0 in ϵ, between libration and circulation motions even for more general systems. In Fig. 2.4 we show the FLI value at $t = 1000$, obtained for a set of 900×900 orbits of the standard map with $\epsilon = 0.3$ and with $I(0)$ and $\varphi(0)$ regularly spaced in the interval $[-\pi : \pi]$. We have considered 2 orthogonal initial vectors $v(0) = (1, 0)$ and $w(0) = (0, 1)$ and we have computed the FLI value using Eq. (2.7) on both vectors; we plot the largest between the two FLI values. When compared with Fig. 2.1 we clearly see that the three different dynamics are well distinguished: the largest FLI values corresponding to chaotic motions, the intermediate values to circulation orbits and the lower values to libration orbits. In [4] it was shown on a pendulum problem that some spurious pattern appear when using FLI (their Fig. 3). We notice that considering the largest between the two FLI values obtained on orthogonal initial vectors, there are no spurious structures in the FLI computation shown in Fig. 2.4.

2.2.2 The Choice of the Integration Time

A second frequently asked question concerns the choice of the integration time. A practical way to choose a suitable integration time is to compute the FLI for different time values and see for which time the picture gets stable. For example,

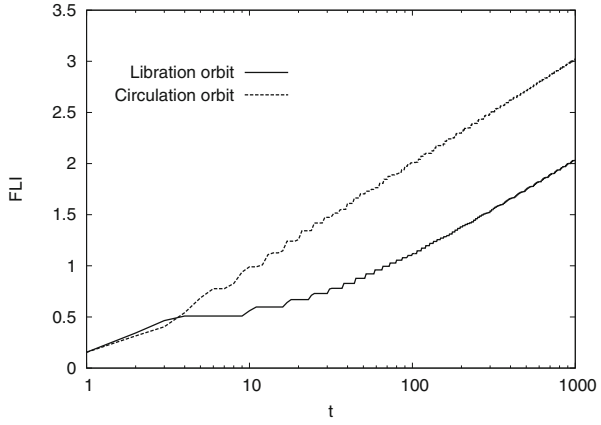

Fig. 2.3 Time evolution of the FLI for the circulation orbit and the libration orbit of Fig. 2.2. The FLI is computed as in (2.7). When considering the supremum of $\log ||v(t)||$ the fluctuations, which are due to the geometry of the orbits, become negligible and libration motion is well distinguished from circulation

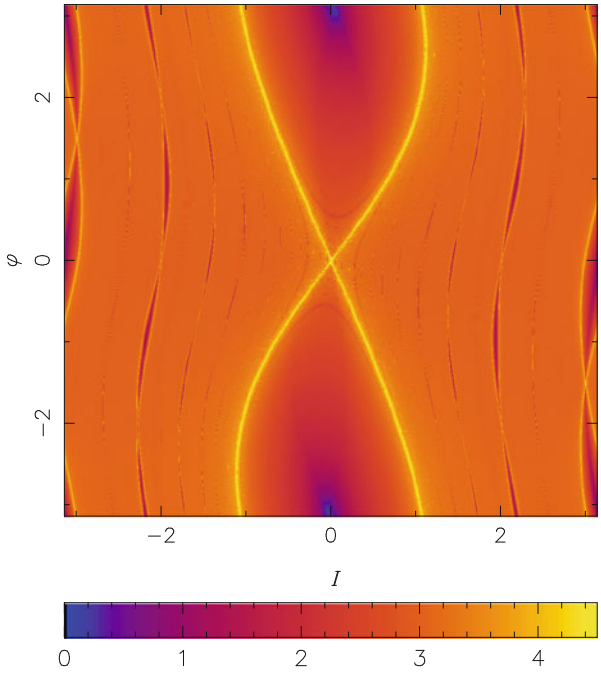

Fig. 2.4 Computation of the FLI for $t = 1000$ using Eq. (2.7) on a grid of 900×900 initial conditions regularly spaced in the interval $[-\pi : \pi]$. Precisely, two FLIs have been computed on 2 orthogonal initial vectors $v(0) = (1, 0)$ and $w(0) = (0, 1)$, the largest FLI value is plotted

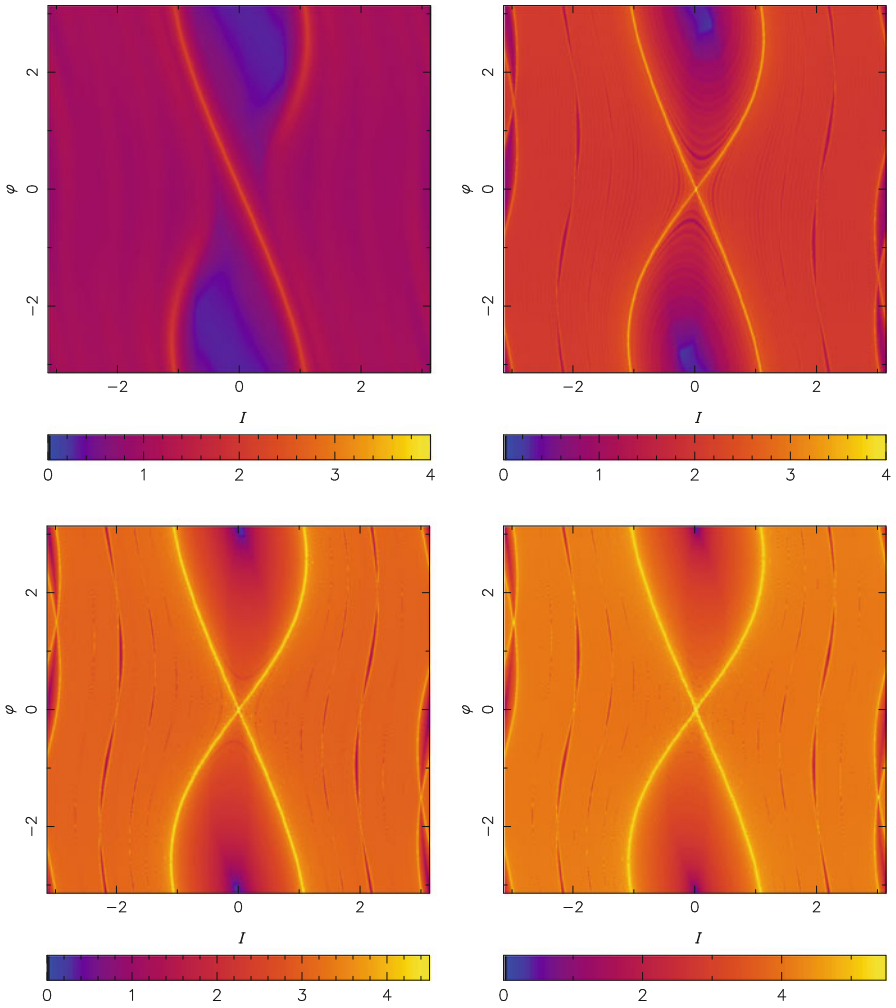

Fig. 2.5 Computation of the FLI as in Fig. 2.4 at $t = 10$ (*top left*), $t = 100$ (*top right*), $t = 1000$ (*bottom left*), $t = 10{,}000$ (*bottom right*)

let's consider the FLI computation shown in Fig. 2.4 for different times, say $t = 10, 100, 1000, 10{,}000$. We see clearly on Fig. 2.5 that $t = 10$ is a too short time to distinguish the dynamics while already at $t = 100$ we clearly distinguish between the different motions. Few more weakly chaotic orbits are detected at $t = 1000$ and no difference appears between $t = 1000$ and $t = 10{,}000$. For this case, $t = 1000$ has to be considered a suitable integration time.

We remark that, the FLI chart obtained in [14] on the relatively short time $t \simeq 1000$ provided a representation of the geometry of the resonances which allowed to follow the diffusion of orbits up to the very long times $t \simeq 10^{11}$.

For further details about the sensitivity of the method in detecting high order resonances we refer to [21].

2.3 The FLI for the Computation of the Stable and Unstable Manifolds

Since the work of Poincaré it is well known that the complexity of chaotic motions in deterministic systems can be appreciated from the analysis of the stable and unstable manifolds associated to hyperbolic orbits. Different methods can be found in the literature for the detection of hyperbolic manifolds. The FLI method for the computation of the hyperbolic manifolds has been introduced in [13, 17, 54] and used in [24, 25, 39, 40] to investigate the relation between the topology of hyperbolic manifolds and diffusion. Recently, the method has been used for the detection of the tube manifolds related to the Lyapunov periodic orbits [41] and for the detection of multiple close encounters [19] in the case of the restricted planar three body problem. We do not enter in the details here, we just recall that we have recently provided [20] an analytic description of the growth of tangent vectors for orbits with initial conditions which are close to the stable-unstable manifolds of a hyperbolic saddle point; as a matter of fact, we explain why the Fast Lyapunov Indicator detects the stable-unstable manifolds of all fixed points which satisfy a certain condition and we provide a suitably modified Fast Lyapunov Indicator if the condition is not satisfied.

Here we illustrate the use of the FLI in detecting hyperbolic manifolds associated to the hyperbolic point $(0, 0)$ on the standard map of Eq. (2.6). Let us recall that the for a two-dimensional standard map the unstable manifold $W_u(I_h, \varphi_h)$ of an hyperbolic point $(I_h, \varphi_h) \in \mathbb{R} \times \mathbb{S}^1$ is the set of (I, φ) such that:

$$W_u(I_h, \varphi_h) = \{(I(0), \varphi(0)) : \lim_{t \to \infty} d((I_h, \varphi_h), (I(-t), \varphi(-t))) = 0\},$$

the stable manifold $W_s(I_h, \varphi_h)$, is the set of (I, φ) such that:

$$W_s(I_h, \varphi_h) = \{(I(0), \varphi(0)) : \lim_{t \to \infty} d((I_h, \varphi_h), (I(t), \varphi(t))) = 0\}.$$

The numerical localization of the unstable manifold of an hyperbolic fixed point can be obtained by propagating a small neighborhood of initial conditions up to a time T of the order of some Lyapunov times of the fixed point (see [40] and references therein). In such a way, one directly constructs a neighborhood of a finite piece of the unstable manifold (for the stable manifold one repeats the construction for the inverse flow). This method gives very good results for fixed points of two dimensional maps, because the neighborhoods of the fixed points are two dimensional and can be propagated with reasonable CPU times. Figure 2.6, left panel shows the detection of a piece of the stable and of the unstable manifolds of the standard map of Eq. (2.6) for $\epsilon = 0.3$. Figure 2.6, right panel shows the value of the FLI obtained on a two dimensional grid of regularly spaced initial conditions

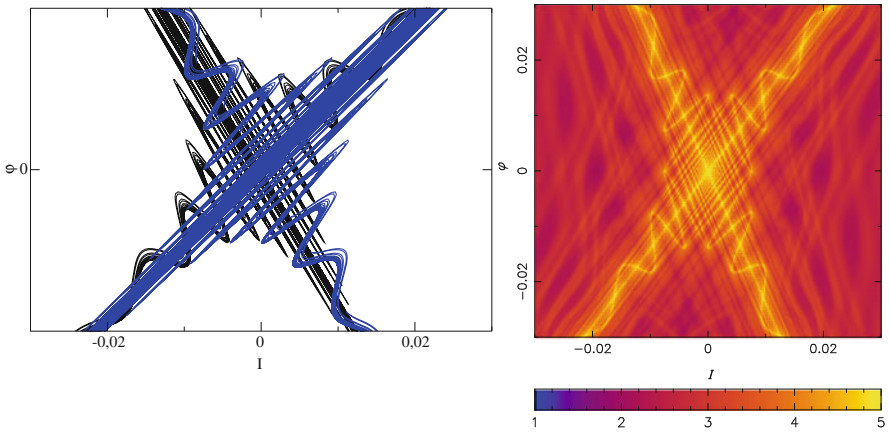

Fig. 2.6 *Left panel*: Detection of a piece of the stable and unstable manifold of the standard map computed with the usual method of set propagation (see [40] and references therein). *Right panel*: Representation of the FLI for the standard map (2.6) for $t = 50$. Precisely, we plot the average of two FLIs obtained on the direct and on the inverse map. We can appreciate the details of the lobes associated to the hyperbolic manifolds and the agreement with the results of the usual method of set propagation

for a short integration time $t = 50$. Precisely, two FLIs have been computed one on the direct and one on the inverse map, and the average of the two FLIs is plotted. We can appreciate the details of the lobes associated to the hyperbolic manifolds. The comparison with Fig. 2.6, left panel shows the quality of the detection of pieces of hyperbolic manifolds as obtained with the FLI computation. The advantage is that the use of the FLI method easily extends to higher dimensional systems and moreover one does not need to know in advance the local approximations of the hyperbolic manifolds.

2.4 Application to a Continuous System

The FLI is easily implemented also for generic continuous dynamical systems. We consider here, as an example, the computation of the FLI for a particle in an accelerated logarithmic potential which models the mean motion of stars in a flat rotation curve galaxy that sustains an asymmetric jet, whose dynamics has been previously studied in [47] using the traditional method of Poincaré surface of sections. The problem of the influence of stellar jets on the dynamics of protoplanetary discs was studied in [44–46]. In [47] the motion of stars in a flat rotation curve galaxy that sustains wind episodes was modeled by:

$$H(\rho, z, p_\rho, p_z) = \frac{1}{2}(p_\rho^2 + p_z^2) + \frac{h_z^2}{2\rho^2} + \frac{1}{2}\log(\rho^2 + z^2) - z \tag{2.8}$$

where ρ and z are the cylindrical coordinates of the star in a reference frame with origin on the galactic center, p_ρ and p_z are the corresponding conjugate momenta, h_z is the projection of the angular momentum along the direction of acceleration (the z-axis). H and h_z are constants of motion of the system. In order to numerically compute the FLI, we integrate the Hamilton equations of (2.8) with a symplectic integrator and we write the variational equations of the map representing the numerical integrator. When dealing with multi-dimensional systems it is evident that we can't visualize the whole phase space as we did for the 2-dimensional standard map. However, we can still provide a global view of the dynamics on suitably chosen 2-dimensional sections. Precisely, the surface of constant energy H is three dimensional, and we can further reduce the study to a two dimensional space by fixing the value of one of the three independent variables.

Figure 2.7 shows the FLI computed on a bidimensional grid of 1000×1000 initial conditions regularly spaced in ρ and z for $E = -0.75$ and $h_z^2 = 0.05831$ with integration time $t = 200$. The other initial conditions are $p_z = 0$ and p_ρ is

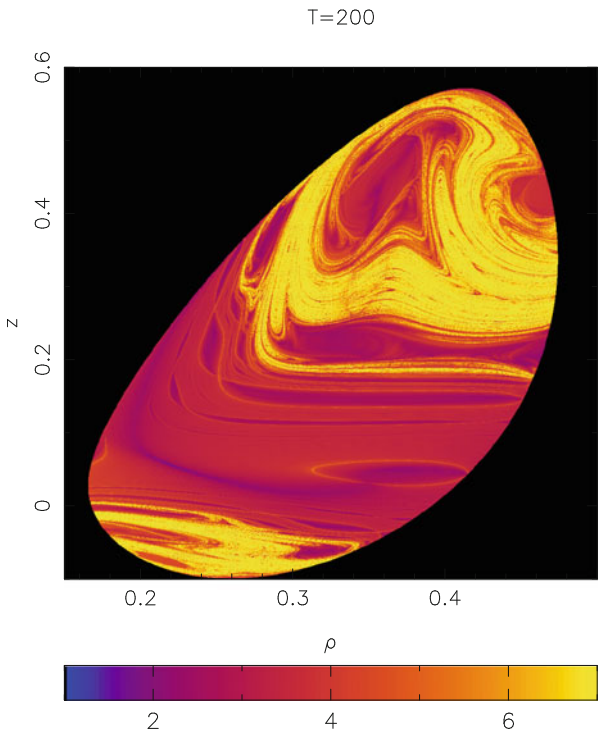

Fig. 2.7 FLI computation of 1000×1000 initial conditions regularly spaced in ρ and z for $H = -0.75$ and $h_z^2 = 0.05831$ with integration time $t = 200$. The other initial conditions are $p_z = 0$ and p_ρ is obtained from the energy equation. For all initial conditions we have chosen $v(0) = (1, 1, 0.5(\sqrt{5} - 1), 1)$

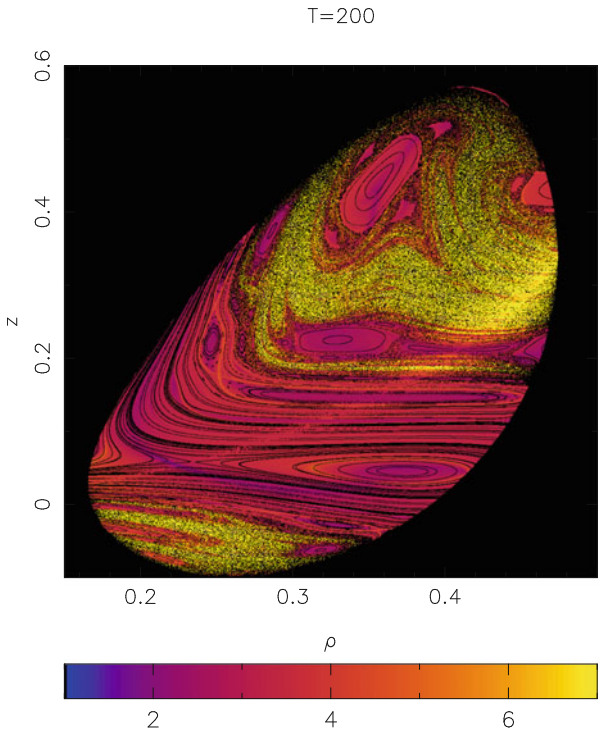

Fig. 2.8 FLI computation as in Fig. 2.7. To compare the results obtained with the FLI to those of the traditional method of surface of section we have drawn with *black points* the intersections of a set of orbits with the plane ρ, z obtained setting $p_z = 0$

obtained from (2.8). For all initial conditions we have chosen $v(0) = (1, 1, 0.5 (\sqrt{5} - 1), 1)$.

We now compare the result of the FLI computation with the results obtained with the traditional method of surface of section. In Fig. 2.8 we plot with black points the intersections of a set of orbits with the plane ρ, z obtained setting $p_z = 0$. We can observe that, as usual, the larger FLI values correspond to chaotic orbits (dispersed points on the surface of section) while intermediate and lower FLI values provide regular motions (closed curves on the surface of section). For the specific case of $H = -0.75$ and $h_z^2 = 0.05831$ the system has a large chaotic region for smaller and larger elevations z. Moreover, using the FLI, we do not only recover the results in [47] concerning the integrability, but we easily obtain much more details in the dynamics. This appears clearly in Fig. 2.9 where the FLI is computed zooming out Fig. 2.7 and we can see the complexity of the chaotic structures. In the bottom part of the figure (for ρ close to 0.25) we recognize the typical lobes related to the hyperbolic manifold of hyperbolic periodic orbits.

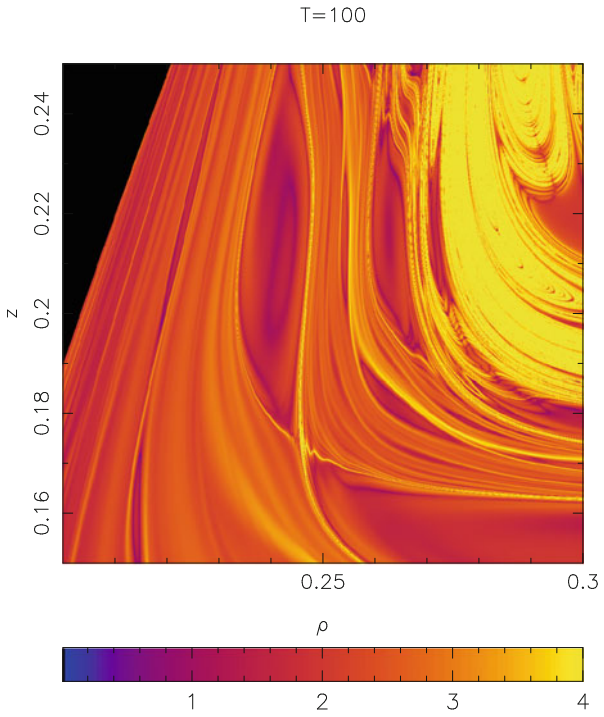

Fig. 2.9 Zoom of Fig. 2.7. The FLI is computed for 1000×1000 initial conditions regularly spaced in ρ and z for $H = -0.75$ and $h_z^2 = 0.05831$ with integration time $t = 100$

2.5 The FLI for Detecting the Geography of Resonances

The problem of long term stability of an Hamiltonian system is strongly related to the famous KAM [1, 28, 43] and Nekhoroshev [48] theorems which leave the possibility of a slow drift of the orbits on a peculiar subset of the phase space, the so called Arnold's web. The detection of the Arnold's web is therefore the first step to achieve if we are interested in studying the long term stability properties of a system.

We consider the following quasi-integrable hamiltonian (that we studied in several papers, see for example [22, 25, 35]):

$$H_\epsilon = \frac{I_1^2}{2} + \frac{I_2^2}{2} + I_3 + \epsilon f \ , \quad f = \frac{1}{\cos(\varphi_1) + \cos(\varphi_2) + \cos(\varphi_3) + 3 + c} \ , \tag{2.9}$$

where ϵ is a small parameter, $c > 0$, and (I, φ) are action angle variables. In the integrable case (defined by $\epsilon = 0$) the actions are constants of motion while the angles $\varphi_1(t) = \varphi_1(0) + I_1 t$, $\varphi_2(t) = \varphi_2(0) + I_2 t$, $\varphi_3(t) = \varphi_3(0) + t$ rotate with frequencies $\omega_1 = I_1$, $\omega_2 = I_2$, $\omega_3 = 1$. Therefore, a couple of actions I_1, I_2

characterizes an invariant torus $\mathbb{T}^3$. For any small ϵ different from zero, H_ϵ is not expected to be integrable. However, if ϵ is sufficiently small, the KAM theorem applies[1]: for any invariant torus of the original system with Diophantine non-resonant frequencies there exists an invariant torus in the perturbed system which is a small deformation of the unperturbed one.

The phase space has dimension 6, therefore, as for the system discussed in Sect. 2.4, we need to properly choose sections in order to provide a visual representation of the dynamics. Since the action I_3 does not enter the equations of motion of all the other variables, we can consider the time evolution in the reduced phase-space $(I_1, I_2, \varphi_1, \varphi_2, \varphi_3)$, and then in this space we consider various sections by fixing the values of some of the variables, for example, we fix the angles and consider the section:

$$S_0 = \{(I_1, I_2, \varphi_1, \varphi_2, \varphi_3) \in \mathbb{R}^2 \times \mathbb{T}^3 : \ \varphi_1, \varphi_2, \varphi_3 = 0\}. \tag{2.10}$$

or, alternatively, we fix one action and two angles and consider the section:

$$S_1 = \{(I_1, I_2, \varphi_1, \varphi_2, \varphi_3) \in \mathbb{R}^2 \times \mathbb{T}^3 : \quad I_2 = I_2(0), \varphi_2, \varphi_3 = 0\} \tag{2.11}$$

or:

$$S_2 = \{(I_1, I_2, \varphi_1, \varphi_2, \varphi_3) \in \mathbb{R}^2 \times \mathbb{T}^3 : \quad I_1 = I_1(0), \varphi_2, \varphi_3 = 0\}. \tag{2.12}$$

In Fig. 2.10 we show the FLI computed for the three different sections S_0, S_1, S_2 represented in the three dimensional space (I_1, I_2, φ_1). Precisely, in the horizontal plane we have represented the FLI computed on section S_0 using a grid of 500×500 initial conditions regularly spaced in (I_1, I_2) in the interval $[-0.5, 1.5]$; on the vertical plane on the left (right) we have represented the FLI computed on section S_1 (S_2) using a grid of 500×500 initial conditions regularly spaced in (I_1, φ_1) (respectively (I_2, φ_1)) in the intervals $[-0.5, 1.5]$ and $[0, 2\pi]$, with respectively $I_2(0) = 1.5, I_1(0) = 1.5$.

In the horizontal plane we clearly see a web of resonance, located near the straight lines defined by: $k_1\omega_1 + k_2\omega_2 + k_3 \equiv k_1 I_1 + k_2 I_2 + k_3 = 0$, with $k_1, k_2, k_3 \in \mathbb{Z}\backslash 0$. For examples the resonances $I_1 = 0$ and $I_2 = 0$ appear as large lines in the horizontal plane. They both have a chaotic boundary (shown in yellow). When looking at the vertical panels it appears clearly that the amplitude of the resonances change with values of the angles.

We now study the evolution of a set of $N = 100$ chaotic orbits with initial conditions $I_1(i) = 1.5, I_2(i) = 0, \varphi_2(i) = \varphi_3(i) = 0, \varphi_1 = \pi + 10^{-6} i, i = 1, ...N$. The orbits evolve in a multi dimensional space, therefore it is useful to consider the points of the orbits intersecting two dimensional sections. On the FLI map of Fig. 2.11 we plot as black dots the points of the orbits which have returned after

[1] H_ϵ is real analytic and H_0 is isoenergetically non-degenerate.

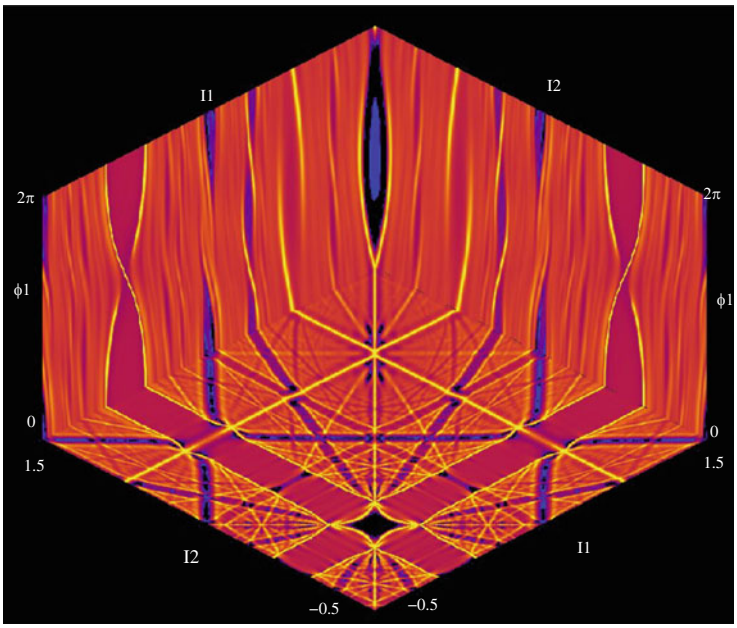

Fig. 2.10 FLI computation for the Hamiltonian of Eq. (2.9) for a value of the perturbing parameter $\epsilon = 0.04$. The integration time is $t = 100$. The initial conditions are regularly spaced on grids of 500×500 points on three different sections of the phase space defined in the text as S_0 (*horizontal plane*), S_1 (*vertical left plane*) and S_2 (*vertical right plane*)

some time on the sections S_2 and S_0. Of course, since computed orbits are discrete, we represent the points that return in a small neighbourhood of S_0 defined by

$$\tilde{S}_0 = \{(I_1, I_2, \varphi_1, \varphi_2, \varphi_3) : \ |\varphi_1| \leq 0.05, |\varphi_2| \leq 0.05, \varphi_3 = 0\}$$

and those that return in a small neighbourhood of S_2 defined by

$$\tilde{S}_2 = \{(I_1, I_2, \varphi_1, \varphi_2, \varphi_3) : \ |\varphi_1| \leq 0.05, |I_1 - 1.5| < 0.005, \varphi_3 = 0\}.$$

Reducing the size of the neighborhood of the sections S_0 and S_2 reduce the number of points but doesn't change the results. In Fig. 2.11 we consider three different integration times: $t = 2\,10^5$ (left panel), $t = 2\,10^7$ (middle panel), $t = 2\,10^8$ (right panel).

On the vertical plane the black points cover the whole chaotic region associated to the chaotic border of the resonance $I_2 = 0$ already on short times. As we can observe in Fig. 2.11 the number of points returning in $\tilde{S}_2$ increases with time but the region covered by the orbits doesn't change.

On the horizontal plane, it is interesting to observe that the orbits slowly diffuse along the resonance $I_2 = 0$, precisely the points that return in $\tilde{S}_0$ cover a portion

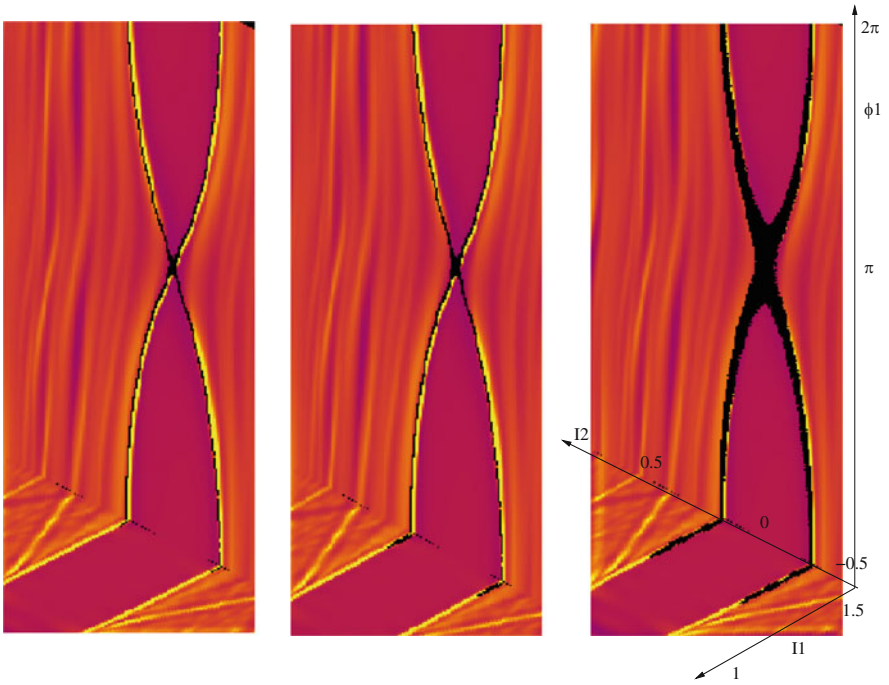

Fig. 2.11 Zoom of Fig. 2.10 around the resonance $I_2 = 0$. We plot as *black dots* the points of a set of $N = 100$ chaotic orbits which have returned after some time on the sections S_2 and S_0. Precisely, we represent the points that return in a small neighbourhood of S_0 defined by $\tilde{S}_0 = \{(I_1, I_2, \varphi_1, \varphi_2, \varphi_3) : \ |\varphi_1| \leq 0.05, |\varphi_2| \leq 0.05, \varphi_3 = 0\}$ and those that return in a small neighbourhood of S_2 defined by $\tilde{S}_2 = \{(I_1, I_2, \varphi_1, \varphi_2, \varphi_3) : \ |\varphi_1| \leq 0.05, |I_1 - 1.5| < 0.005, \varphi_3 = 0\}$. The three panels correspond to different integrations times: $t = 2\,10^5$ (*left panel*), $t = 2\,10^7$ (*middle panel*) and $t = 2\,10^8$ (*right panel*). The initial conditions are chosen in the neighbourhood of the hyperbolic point: $I_1(i) = 1.5, I_2(i) = 0, \varphi_2(i) = \varphi_3(i) = 0, \varphi_1 = \pi + 10^{-6} i, i = 1, ...N$

of the chaotic border of the resonance that increases for increasing values of the integration time. Let us remark that the FLI, computed on a short total time $t = 100$, allows to properly follow orbits on a much larger integration time ($t = 2\,10^8$ on the right panel of Fig. 2.11).

Let us remark that the section S_0 is particularly suited to the detection of the slow diffusion since the large oscillations of the action I_2 that we observe on section S_2 are filtered when considering the points that return in $\tilde{S}_0$. Moreover, the FLI chart allows us to check that the orbits really diffuse along the chaotic border of a resonance.

We have quantified the diffusion by measuring a diffusion coefficient using the points of sets of orbits returning in the section $\tilde{S}_0$ using various Hamiltonian or discrete mapping models in [14, 18, 22, 24–26, 35, 36]. The computation of the diffusion coefficient has many technical difficulties that we do not recall here. The interested reader can refer to [25] for a numerical characterization of the statistical

properties of the diffusion and to [18] for the technical aspects of the computation of the diffusion coefficient.

In [22] we have shown that the diffusion of orbits occurring along the peculiar set of resonances has a global character and in [26] we measured a diffusion coefficient decreasing exponentially through 40 orders of magnitude thus showing that Arnold's diffusion concerns and can be measured on systems of physical interest.

2.6 Conclusions

Since the pioneering work of Hénon and Heiles [27] it appeared clearly that understanding the dynamical behaviours of a system required global studies of the phase space. Different tools for the detection of chaotic and ordered motions have been developed since then, providing interesting results in different domains of physics (celestial mechanics, particle accelerators, dynamical astronomy, statistical physics, plasma physics). The Fast Lyapunov Indicator was introduced in [12] as an easy (to implement) and sensitive tool for distinguish between ordered and chaotic motion. The method was used in [13] for the detection of the Arnold web of a system and further developed in [21] using a refined perturbation theory which provided the behaviour of the FLI for different orbits.

In the last 10 years we have used the FLI for studies for which a global visualization of the phase space was one of the key ingredients for understanding the problem. For example, the Arnold web computed with short integration time allowed us to choose possibly diffusing initial conditions and to follow their evolution on much longer integration time. With a rather technical method we have measured diffusion coefficients decreasing faster than a power low and possibly exponentially through many orders of magnitude [14, 18, 22, 24–26, 35, 36] showing the interest of Arnold's diffusion for physical systems.

Later in [17, 24, 38–40] we have used the FLI for the detection of the stable and unstable manifolds. This is in general a difficult task that requires sophisticated methods. We have recently provided [20] an analytic description of the growth of tangent vectors for orbits with initial conditions which are close to the stable-unstable manifolds of a hyperbolic saddle point and we have explained the condition for the detection the stable-unstable manifolds with the FLI.

Moreover, the FLI has been applied to the planar circular restricted three body problem for the detection and characterization of close encounters and resonances [19, 41].

In this chapter we have we presented the indicator for readers that would like to implement it for the first time. At this purpose we have chosen simple discrete and continuous model problems giving the element to reproduce this cases. As examples of applications we have shown (1) the use of the FLI for the detection of the stable/unstable manifold of a two dimensional model, (2) the FLI for the

detection of the resonances of continuous systems and (3) we have explained how to use the indicator to follow the diffusion of orbits along resonant lines.

References

1. Arnold, V.I.: Proof of a theorem by A.N. Kolmogorov on the invariance of quasi-periodic motions under small perturbations of the Hamiltonian. Russ. Math. Surv. **18**, 9 (1963)
2. Arnold, V.I.: Instability of dynamical systems with several degrees of freedom. Sov. Math. Dokl. **6**, 581–585 (1964)
3. Barrio, R.: Sensitivity tools vs. Poincaré sections. Chaos Solitons Fractals **25**, 711–726 (2005)
4. Barrio, R., Borczyk, W., Breiter, S.: Spurious structures in chaos indicators maps. Chaos Solitons Fractals **40**, 1697–1714 (2009)
5. Celletti, A., Froeschlé, C., Lega, E.: Dissipative and weakly-dissipative regimes in nearly-integrable mappings. Discrete Contin. Dyn. Syst. Ser. A **16**(4), 757–781 (2006)
6. Celletti, A., Froeschlé, C., Lega, E.: Dynamics of the conservative and dissipative spin–orbit problem. Planet. Space Sci. **55**, 889–899 (2007)
7. Celletti, A., Stefanelli, L., Lega, E., Froeschlé, C.: Global dynamics of the regularized restricted three-body problem with dissipation. Celest. Mech. Dyn. Astron. **109**, 265–284 (2011)
8. Cincotta, P.M., Simó, C.: Simple tools to study global dynamics in non-axisymmetric galactic potentials - I. Astron. Astrophys. Suppl. Ser. **147**, 205 (2000)
9. Cincotta, P.M., Giordano, C.M., Simó, C.: Phase space structure of multi-dimensional systems by means of the mean exponential growth factor of nearby orbits. Physica D **182**(3–4), 151–178 (2003)
10. Froeschlé, C., Lega, E.: Weak chaos and diffusion in Hamiltonian systems. From Nekhoroshev to Kirkwood. In: Roy, A.E. (eds.) The Dynamics of Small Bodies in the Solar System: A Major Key to Solar System Studies. NATO/ASI. Kluwer Academic, Boston (1998)
11. Froeschlé, C., Lega, E.: On the structure of symplectic mappings. The fast Lyapunov indicator: a very sensitive tool. Celest. Mech. Dyn. Astron. **78**(1/4), 167–195 (2000)
12. Froeschlé, C., Lega, E., Gonczi, R.: Fast Lyapunov indicators. Application to asteroidal motion. Celest. Mech. Dyn. Astron. **67**, 41–62 (1997)
13. Froeschlé, C., Guzzo, M., Lega, E.: Graphical evolution of the Arnold web: from order to chaos. Science **289**(5487), 2108–2110 (2000)
14. Froeschlé, C., Guzzo, M., Lega, E.: Local and global diffusion along resonant lines in discrete quasi-integrable dynamical systems. Celest. Mech. Dyn. Astron. **92**(1–3), 243–255 (2005)
15. Guzzo, M.: The web of three-planets resonances in the outer solar system. Icarus **174**(1), 273–284 (2005)
16. Guzzo, M.: The web of three-planet resonances in the outer solar system II: a source of orbital instability for Uranus and Neptune. Icarus **181**, 475–485 (2006)
17. Guzzo, M.: Chaos and diffusion in dynamical systems through stable–unstable manifolds. In: Perozzi, Mello, F. (eds.) Space Manifolds Dynamics: Novel Spaceways for Science and Exploration. Novel Spaceways for scientific and exploration missions, a dynamical systems approach to affordable and sustainable space applications held in Fucino Space Centre (Avezzano), 15–17 October 2007. Springer, New York/Dordrecht/Heidelberg/London (2010)
18. Guzzo, M., Lega, E.: The numerical detection of the Arnold web and its use for long-term diffusion studies in conservative and weakly dissipative systems. Chaos **23**, 23124 (2013)
19. Guzzo, M., Lega, E.: On the identification of multiple close encounters in the planar circular restricted three-body problem. Mon. Not. R. Astron. Soc. Lett. **428**, 2688–2694 (2013)
20. Guzzo, M., Lega, E.: Evolution of the tangent vectors and localization of the stable and unstable manifolds of hyperbolic orbits by Fast Lyapunov Indicators. SIAM J. Appl. Math. **74**(4), 1058–1086 (2014)

21. Guzzo, M., Lega, E., Froeschlé, C.: On the numerical detection of the effective stability of chaotic motions in quasi-integrable systems. Physica D **163**(1–2), 1–25 (2002)
22. Guzzo, M., Lega, E., Froeschlé, C.: First numerical evidence of Arnold diffusion in quasi-integrable systems. Discrete Continuous Dyn. Syst. Ser. B **5**(3), 687–698 (2005)
23. Guzzo, M., Lega, E., Froeschlé, C.: Diffusion and stability in perturbed non-convex integrable systems. Nonlinearity **19**, 1049–1067 (2006)
24. Guzzo, M., Lega, E., Froeschlé, C.: A numerical study of the topology of normally hyperbolic invariant manifolds supporting Arnold diffusion in quasi-integrable systems. Physica D **238**, 1797–1807 (2009)
25. Guzzo, M., Lega, E., Froeschlé, C.: A numerical study of Arnold diffusion in a priori unstable systems. Commun. Math. Phys. **290**, 557–576 (2009)
26. Guzzo, M., Lega, E., Froeschlé, C.: First numerical investigation of a conjecture by N.N. Nekhoroshev about stability in quasi-integrable systems. Chaos **21**(3), 033101-1–033101-12 (2011)
27. Hénon, M., Heiles, C.: The applicability of the third integral of motion: some numerical experiments. Astron. J. **69**, 73–79 (1964)
28. Kolmogorov, A.N.: On the conservation of conditionally periodic motions under small perturbation of the Hamiltonian. Dokl. Akad. Nauk. SSSR **98**, 527–530 (1954)
29. Laskar, J.: The chaotic motion of the Solar system. A numerical estimate of the size of the chaotic zones. Icarus **88**, 266–291 (1990)
30. Laskar, J.: Frequency analysis for multi-dimensional systems. Global dynamics and diffusion. Physica D **67**, 257–281 (1993)
31. Laskar, J., Froeschlé, C., Celletti, A.: The measure of chaos by the numerical analysis of the fundamental frequencies. Application to the standard mapping. Physica D **56**, 253 (1992)
32. Lega, E., Froeschlé, C.: Fast Lyapunov Indicators. Comparison with other chaos indicators. Application to two and four dimensional maps. In: Henrard, J., Dvorak, R. (eds.) The Dynamical Behaviour of our Planetary System. Springer, The Netherlands (1997)
33. Lega, E., Froeschlé, C.: Comparison of convergence towards invariant distributions for rotation angles, twist angles and local Lyapunov characteristic numbers. Planet. Space Sci. **46**, 1525–1534 (1998)
34. Lega, E., Froeschlé, C.: On the relationship between fast Lyapunov indicator and periodic orbits for symplectic mappings. Celest. Mech. Dyn. Astron. **81**, 129–147 (2001)
35. Lega, E., Guzzo, M., Froeschlé, C.: Physica D **182**, 179–187 (2003)
36. Lega, E., Froeschlé, C., Guzzo, M.: Diffusion in Hamiltonian quasi-integrable systems. In: Benest, D., Froeschlé, C., Lega, E. (eds.) Topics in Gravitational Dynamics. Lecture Notes in Physics, vol. 729. Springer, Berlin (2007)
37. Lega, E., Guzzo, M., Froeschlé, C.: Measure of the exponential splitting of the homoclinic tangle in four dimensional symplectic mappings. Celest. Mech. Dyn. Astron. **104**, 191–204 (2009)
38. Lega, E., Guzzo, M., Froeschlé, C.: A numerical study of the size of the homoclinic tangle of hyperbolic tori and its correlation with Arnold diffusion in Hamiltonian systems. Celest. Mech. Dyn. Astron. **107**, 129–144 (2010)
39. Lega, E., Guzzo, M., Froeschlé, C.: A numerical study of the hyperbolic manifolds in a priori unstable systems. A comparison with Melnikov approximations. Celest. Mech. Dyn. Astron. **107**, 115–127 (2010)
40. Lega, E., Guzzo, M., Froeschlé, C.: Numerical Studies of hyperbolic manifolds supporting diffusion in symplectic mappings. Eur. Phys. J. Spec. Top. **186**, 3–31 (2010)
41. Lega, E., Guzzo, M., Froeschlé, C.: Detection of Close encounters and resonances in three body problems through Levi-Civita regularization. Mon. Not. R. Astron. Soc. Lett. **418**, 107–113 (2011)
42. Mitchenko, T.A., Ferraz–Mello, S.: Astron. J. **122**, 474–481 (2001)
43. Moser, J.: On invariant curves of area-preserving maps of an annulus. Commun. Pure Appl. Math. **11**, 81–114 (1958)
44. Namouni, F.: Astron. J. **130**, 280 (2005)

45. Namouni, F.: LNP **729**, 233 (2007)
46. Namouni, F., Guzzo, M.: Celest. Mech. Dyn. Astron. **99**, 31 (2007)
47. Namouni, F., Guzzo, M., Lega, E.: On the integrability of stellar motion in an accelerated logarithmic potential. Astron. Astrophys. **489**, 1363 (2008)
48. Nekhoroshev, N.N.: Exponential estimates of the stability time of near-integrable Hamiltonian systems. Russ. Math. Surv. **32**, 1–65 (1977)
49. Robutel, P.: Frequency map analysis and quasiperiodic decompositions. In: Benest et al. (eds.) Hamiltonian Systems and Fourier Analysis, pp. 179–198. Taylor and Francis. Adv. Astron. Astrophys., Cambridge Sci. Publ., Cambridge (2005)
50. Robutel, P., Galern, F.: The resonant structure of Jupiter's Trojan asteroids I. Long term stability and diffusion. Mon. Not. R. Astron. Soc. **372**, 1463–1482 (2006)
51. Robutel, P., Laskar, J.: Frequency map and global dynamics in the Solar System I. Icarus **52**(1), 4–28 (2001)
52. Tang, X.Z., Boozer, A.H.: Finite time Lyapunov exponent and advection-diffusion equation. Physica D **95**(3–4), 283–305 (1996)
53. Todorović, N., Guzzo, M., Lega, E., Froeschlé, C.: A numerical study of the stabilization effect of steepness. Celest. Mech. Dyn. Astron. **110**(4), 389–398 (2011)
54. Villac, B.F.: Using FLI maps for preliminary spacecraft trajectory design in multi-body environments. Celest. Mech. Dyn. Astron. **102**, 29–48 (2008)
55. Wayne, B.H., Malykh, A.V., Danforth, C.M.: The interplay of chaos between the terrestrial and giant planets. Mon. Not. R. Astron. Soc. **407**(3), 1859–1865 (2010)